JOURNAL OF CATALYSIS 133, 42–54 (1992)

Aggregate Size Effects in ^{129}Xe NMR of Y-Type Zeolites

CATHY TWAY AND TOM APPLE[1]

Department of Chemistry, University of Nebraska–Lincoln, Lincoln, Nebraska, 68588-0304

Received March 26, 1991; revised August 20, 1991

Crystallite aggregates of Na–Y, Ba–Y, Ca–Y, Fe–Y, and Ru–Y zeolites have been studied via ^{129}Xe NMR spectroscopy. The response of the ^{129}Xe resonance of adsorbed xenon depends upon the aggregate size. This effect is observed in Ca–Y, Ru–Y, and Fe–Y zeolites. Both the chemical shift and the linewidth of the ^{129}Xe resonance display a large aggregate size dependence. Differences in linewidths are observed in Ba–Y and Na–Y zeolites. Samples made by mixing Ru–Y zeolite with Na–Y exhibit a motional narrowing, which also depends upon aggregate size. A packing dependence is observed in samples of Fe–Y and in mixed samples containing both Ru–Y and Na–Y. These results are consistent with a model in which xenon atoms migrate over many zeolite crystallites on the NMR timescale. The aggregate size effects are attributed to intercrystalline diffusion and residence of xenon atoms in the mesopore structure occurring at aggregate grain boundaries.

INTRODUCTION

^{129}Xe NMR is becoming a standard technique in the study of solid materials (*1–5*). The ^{129}Xe nucleus is spin-$\frac{1}{2}$, is present in 26.44% natural abundance, and possesses a large chemical shift range. In addition, xenon is unreactive with most materials.

The chemical shift of a ^{129}Xe atom sorbed in a zeolite is dependent upon its interaction with other xenon atoms, framework oxygen atoms, charge-compensating cations, and adsorbed species. Xenon's van der Waals radius of 4.4 Å restricts it to the supercages and the connecting channels. The sodalite units and hexagonal prisms are not directly accessible. Thus, ^{129}Xe NMR can be used to study the location of adsorbed species (*2*) and the migration of metal particles (*3*).

Recently, there has been some question concerning the rate of diffusion of xenon within a zeolite. Self-diffusion coefficients of xenon in Na–X and Ca–A zeolites have been measured using the pulsed field gradient method (*6*). The coefficients are given in Table 1. These values suggest that in Na–X it is possible for xenon to sample many crystallites on the NMR timescale rather than merely a few supercages as was previously assumed (*7*). This calls into question the interpretations of earlier results (*8*). Shoemaker and Apple (*3*) were the first to suggest that rapid intercrystalline diffusion occurs in Ru–Y-type zeolites. They observed partial coalescence of the ^{129}Xe NMR spectrum of a sample containing both reduced Ru–Y and Na–Y mixed on a macroscopic scale. This behavior indicated that xenon was sampling regimes of Ru–Y and Na–Y crystallites on the NMR timescale. This same approach has since been employed by others with similar results in Pt–Y zeolites and other mixed samples (*9, 10*).

In fact, samples of zeolites are actually present as aggregates of many micrometer-size crystals with void spaces between the crystallites forming mesopores. In these samples, there are actually three types of diffusion processes occurring: diffusion of xenon between aggregates, diffusion of xenon within crystallites in a single aggregate, and true intracrystalline diffusion. Up to this point, the interpretation of the NMR spectrum of ^{129}Xe results has not dealt with either

[1] Current address: Chemistry Department, Rensselaer Polytechnic Institute, Troy, NY 12180.

0021-9517/92 $3.00

TABLE 1

Self-Diffusion Coefficients for Xe[a]

Zeolite	Self-diffusion coefficient
Ca–A	2×10^{9} m^2/s
Na–X	7×10^{8} m^2/s

[a] Karger *et al.* (*6*).

diffusion from crystallite to crystallite within an aggregate or diffusion between aggregates even though this type of diffusion has been shown to be a factor in catalysis (*11*). To determine what effect macroporous diffusion has on ^{129}Xe NMR, zeolites of different aggregate size have been studied. Mixing experiments have also been performed with Ru–Y and Na–Y aggregates in order to study the effects of aggregate size.

METHODS

Rinsed Linde LZY-52 molecular sieves were used as the starting material for all samples. Ru–Y zeolite was prepared by ion exchange with 0.04 *M* $RuCl_3$ ($RuCl_3 : 3H_2O$ Strem). After constant stirring for 24 h, the zeolite was washed with deionized H_2O and dried at 385 K for 24 h. The supernatant solutions prior to and following ion exchange were analyzed with atomic absorption and argon plasma emission spectrophotometry. The catalyst was found to be 8.2 ± 0.2% ruthenium by weight. Fe–Y was prepared by using 0.05 *M* solution of $FeCl_3$ ($FeCl_3 : 6H_2O$) and analyzed by Harris Laboratories, Inc. Separate analyses were performed on coarse and fine aggregate samples of Fe–Y. The coarse aggregate Fe–Y was 1.19 ± .04% iron by weight and the fine aggregate sample was 1.25 ± .04% iron by weight. Samples containing 15.5 ± 0.06% barium by weight were prepared from a 0.25 *M* solution of $BaCl_2$ ($BaCl_2 : 2H_2O$). Ca–Y (48% exchanged) was prepared in a similar manner using a 0.05 *M* $CaCl_2$ solution. Na–Y was rinsed with deionized H_2O and treated in an identical manner with all the other samples.

Aggregates were separated using homemade sieves whose sieving capabilities had previously been analyzed using a reflecting microscope. The zeolites were separated into the following classifications: fine aggregates, which were sieved through a 1×10^{-4} m mesh, medium aggregates, which passed a 2×10^{-4} m mesh but not a 1×10^{-4} m mesh, and coarse aggregates, which did not sieve through a 2×10^{-4} m mesh. For convenience, these different sizes will be referred to as fine, medium, and coarse throughout the remainder of this paper. In addition, aggregates were separated by hand from the coarse aggregates of Fe–Y to prepare a sample whose aggregates were much larger than the normal coarse sample. This sample will be referred to as supercoarse.

All samples were evacuated on a glass vacuum system at the specified temperature to a residual pressure of less than 5×10^{-5} Torr (1 Torr = 133.3 N m^{-2}). All reductions were carried out on the same vacuum system under static H_2 (Linde 99.999%), which was dried by passing through Drierite and molecular sieves prior to exposure to the sample. H_2 uptakes were monitored using a capacitance manometer (MKS Instruments, Inc.). Research grade xenon was obtained from Scott Specialty Gases and used without further purification. N_2 isotherms were performed on the same vacuum system using prepurified grade N_2 (Linde), which was dried prior to use.

^{129}Xe spectra were acquired using a Varian VXR-200 NMR spectrometer operating at 55.337 MHz for ^{129}Xe. The number of transients collected ranged from 500 to 7500 depending upon the nature of the cation in the sample and the xenon over pressure. A relaxation delay of 1.0 s was used for all samples. Chemical shifts were referenced to a secondary standard of Xe in Na–Y whose resonance had previously been referenced to that of xenon gas at zero pressure using Jameson's equation (*12*). The magnet was locked in all experiments by using 8-mm-o.d. NMR sample tubes equipped with J. Young valves inserted within 10-mm-o.d.

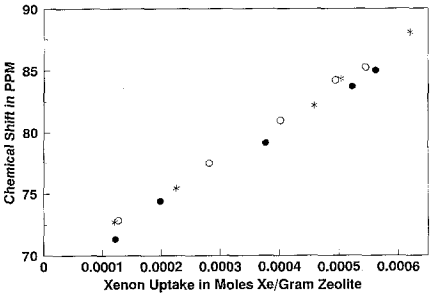

FIG. 1. Plot of xenon chemical shift versus xenon uptake for Na–Y zeolites of various aggregate sizes: ○, coarse; *, medium; ●, fine.

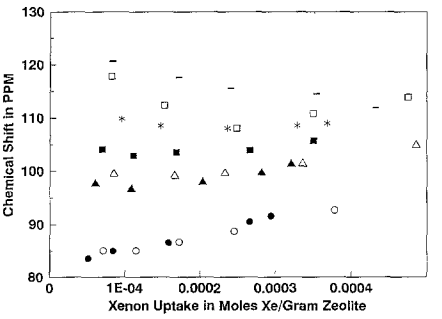

FIG. 3. Plot of xenon chemical shift versus xenon uptake for Ru–Y zeolites of various aggregate sizes (all samples evacuated at 625 K unless otherwise noted): □, coarse; △, coarse, red. 298 K; ○, coarse, red., and evac. 775 K; *, medium; ■, fine; ▲, fine, red. 298 K; ●, fine, red., and evac. 775 K; –, crushed.

NMR tubes filled with D_2O (*9*). Deuterated acetone was used in the low-temperature NMR studies. ^{27}Al NMR was performed at 93.8 MHz with a homebuilt magic-angle spinning probe.

RESULTS

The relationship between the chemical shift and the xenon concentration in the zeolite for Na–Y, Ru–Y, Ba–Y, Ca–Y, and Fe–Y is shown in Figs. 1–5. The effect of crystallite aggregate size on the chemical shift of ^{129}Xe is most apparent for the Ru–Y and Fe–Y samples (Figs. 2, 3), with no significant difference in the Na–Y (Fig. 1). The results for all samples of Na–Y regardless of particle size or sample treatment are in good agreement with earlier published results (*1*, *3*). The ^{129}Xe chemical shifts of the fine aggregate samples of Ru–Y (Fig. 3) show little dependence on xenon uptake; however, increasing concentration dependence is observed as the sample is reduced at higher temperatures. The Ru–Y sample of coarse particle size is in agreement with that of Shoemaker and Apple (*3*). Interestingly, the crushed Ru–Y has chemical shifts similar to those of the coarse sample. No previous studies using ^{129}Xe to study Fe–Y zeolites could be located; however, the coarse particle sample gives the parabolic-shaped relationship that has been observed for other polyvalent cation-exchanged Y-type zeolites (*1*, *3*) and is almost identical in curvature with the Ru–Y coarse sample.

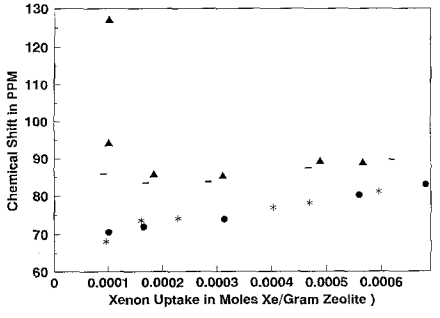

FIG. 2. Plot of xenon chemical shift versus xenon uptake for Fe–Y zeolites of various aggregate sizes: ▲, supercoarse; _, coarse; *, medium; ●, fine.

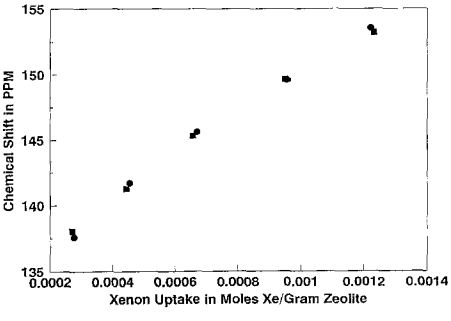

FIG. 4. Plot of xenon chemical shift versus xenon uptake for Ba–Y zeolites of various aggregate sizes: ■, coarse; ●, fine.

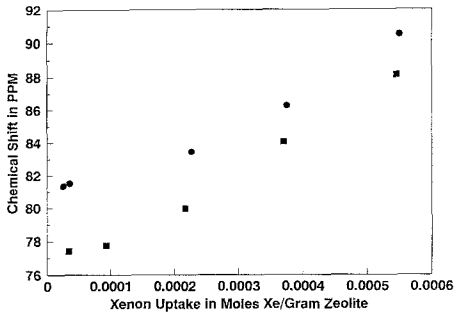

FIG. 5. Plot of xenon chemical shift versus xenon uptake for Ca–Y zeolites of various aggregate sizes: ●, coarse; ■, fine.

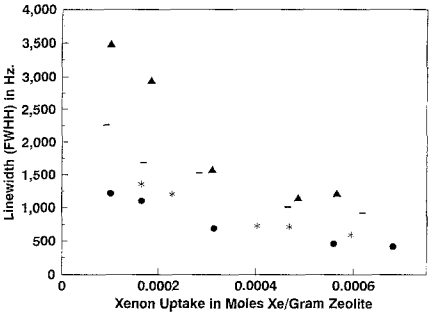

FIG. 7. Plot of xenon linewidth versus xenon uptake for Fe–Y zeolites of various aggregate sizes: ▲, supercoarse; –, coarse; *, medium; ●, fine.

The concentration dependence of the ^{129}Xe resonances in the Fe–Y sample of fine crystallite aggregate size, however, is linear and similar to that of Na–Y (Fig. 2). The results for Ca–Y and Ba–Y samples are in agreement with those of Ito and Fraissard (*1*).

The corresponding linewidths for these ^{129}Xe resonances are shown in Figs. 6–10. For all Y-type zeolite samples studied so far in our laboratory, there is a significant difference between the linewidths of the various crystallite aggregate sizes. The most dramatic difference is that in the Fe–Y samples, the coarser particles are 11–50 ppm wider than those of the fine particles.

The chemical shifts of xenon in these samples are also dependent upon the packing conditions. In a typical sample preparation, a small plug of quartz wool is placed above the zeolite in the tube in order to keep the particles from entering the vacuum line during the evacuation procedures. By placing this plug above the sample, a small amount of packing is inevitable. However, samples of Fe–Y were prepared leaving a large dead space between the sample and the quartz plug, thus leaving the particles more or less unpacked or at the very least very loosely packed. The results for these experiments are shown in Figs. 11 and 12. The xenon resonances in the unpacked samples are deshielded at low xenon concentrations, but become quite similar to those of the normally prepared Fe–Y samples as the xenon concentration increases.

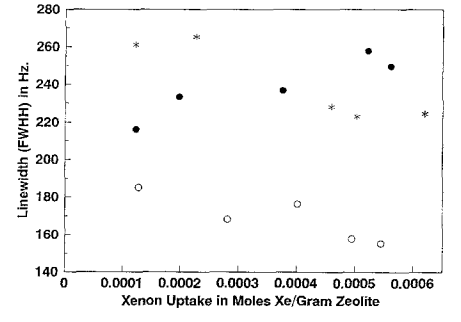

FIG. 6. Plot of xenon linewidth versus xenon uptake for Na–Y zeolites of various aggregate sizes: ○, coarse; *, medium; ●, fine.

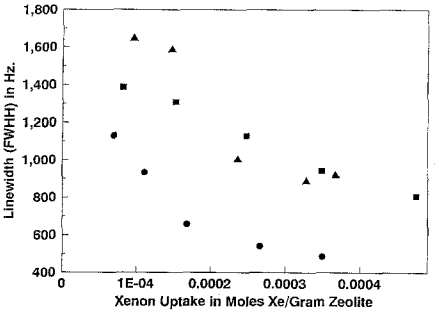

FIG. 8. Plot of xenon linewidth versus xenon uptake for Ru–Y zeolites of various aggregate sizes: ■, coarse; ▲, medium; ●, fine.

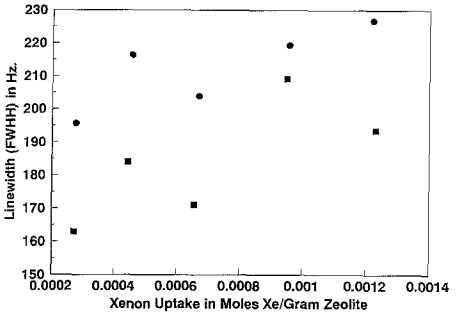

FIG. 9. Plot of xenon linewidth versus xenon uptake for Ba–Y zeolites of various aggregate sizes: ■, coarse; ●, fine.

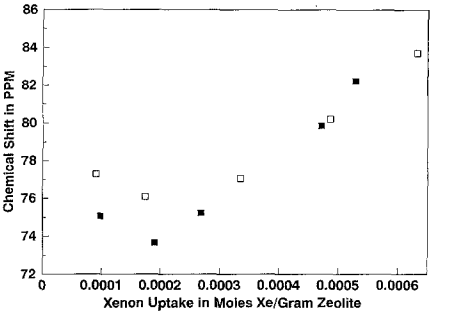

FIG. 11. Plot of xenon chemical shift versus xenon uptake for coarse Fe–Y zeolites with differing packing: □, unpacked; ■, packed.

The packing dependence indicates that the interaggregate volume affects the observed chemical shift of xenon. Similar packing experiments were performed with mixed Ru–Y and Na–Y samples of coarse aggregate size. When the sample is packed, we observe three xenon resonances (Fig. 13): one corresponding to that of coarse Ru–Y in the range 110–120 ppm, one associated with xenon in Na–Y zeolite at 70–80 ppm, and a third intermediate between these two. The third peak is absent when no packing is used during sample preparation.

It is noteworthy that the Ru–Y samples have a much softer texture than other samples studied, and are, therefore, more susceptible to aggregate breakup during packing. ^{27}Al magic-angle spinning NMR of these samples (Fig. 14) reveals that impregnation of the zeolite with $RuCl_3$ causes some dealumination of the lattice as evidenced by the peak at 0 ppm relative to $Al(H_2O)_6$ indicative of octahedral detrital aluminum species. X-ray crystallography of the Ru–Y samples shows some loss of crystallinity; however, this is apparently not simply due to the low pH of the exchange solution. Zeolites that were immersed in HCl solutions of identical pH as the $RuCl_3$ exchange solution show little loss of crystallinity. Thus, the mechanism of dealumination appears to involve Ru. This phenomenon is under further investigation in our laboratory.

The three samples of Ru–Y having various aggregate sizes have different xenon uptakes as shown in Fig. 15. Transmission

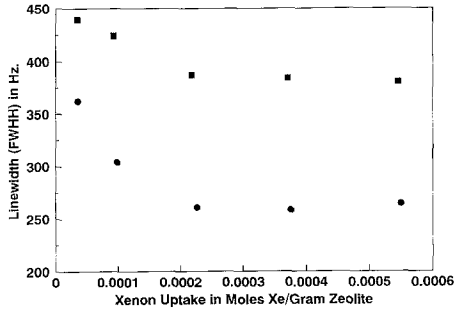

FIG. 10. Plot of xenon linewidth versus xenon uptake for Ca–Y zeolites of various aggregate sizes: ●, coarse; ■, fine.

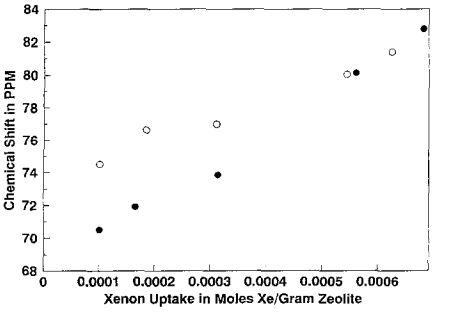

FIG. 12. Plot of xenon chemical shift versus xenon uptake for fine Fe–Y zeolites with differing packing: ○, unpacked; ●, packed.

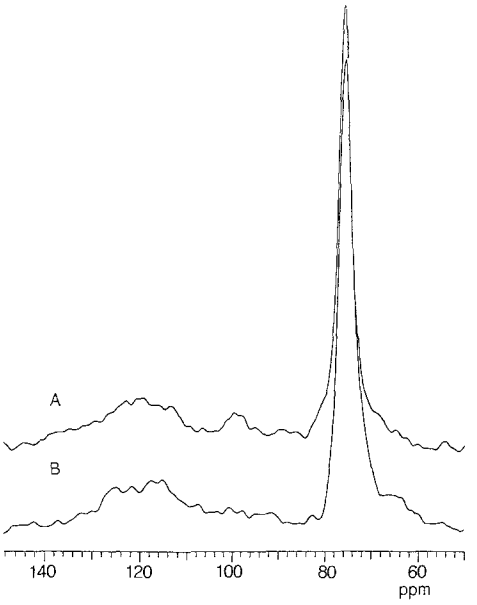

FIG. 13. ^{129}Xe NMR spectra of a mixture of coarse aggregates of Na–Y and Ru–Y zeolites: (A) packed; (B) unpacked.

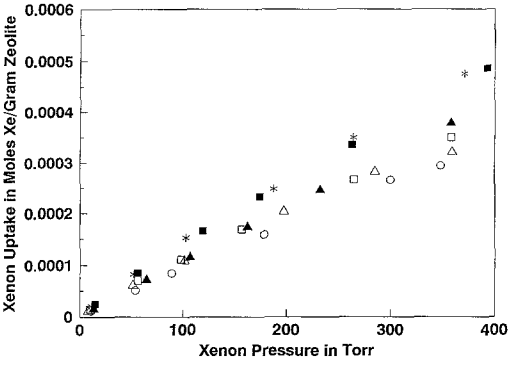

FIG. 15. Plot of xenon uptake versus xenon pressure for Ru–Y zeolite of various aggregate sizes (samples evacuated at 625 K unless otherwise noted): □, fine; △, fine, red. at 298 K; ○, fine, red., and evac. 775 K; *, coarse; ■, coarse, red. 298 K; ▲, coarse red., and evac. 775 K.

electron microscopy indicates the presence of some distorted crystallites that apparently have been created during the ion-exchange process. Sample TEM photographs contrasting Ru–Y to Na–Y zeolite are shown in Fig. 16. We attribute differences in the xenon uptake with aggregate size to the presence of these small damaged crystallites that are more prevalent in the samples of small aggregate size due to sieving. Because this component is not completely crystalline, the xenon uptake in the fine sample is reduced. Lower microporosity values were measured for the fine Ru–Y sample compared to the coarse aggregate sample.

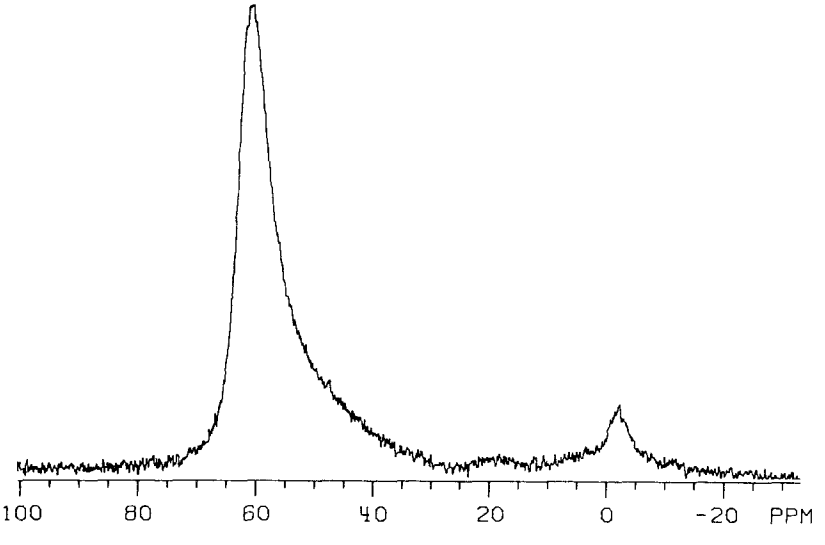

FIG. 14. ^{27}Al MAS NMR spectrum of as-prepared Ru–Y zeolite.

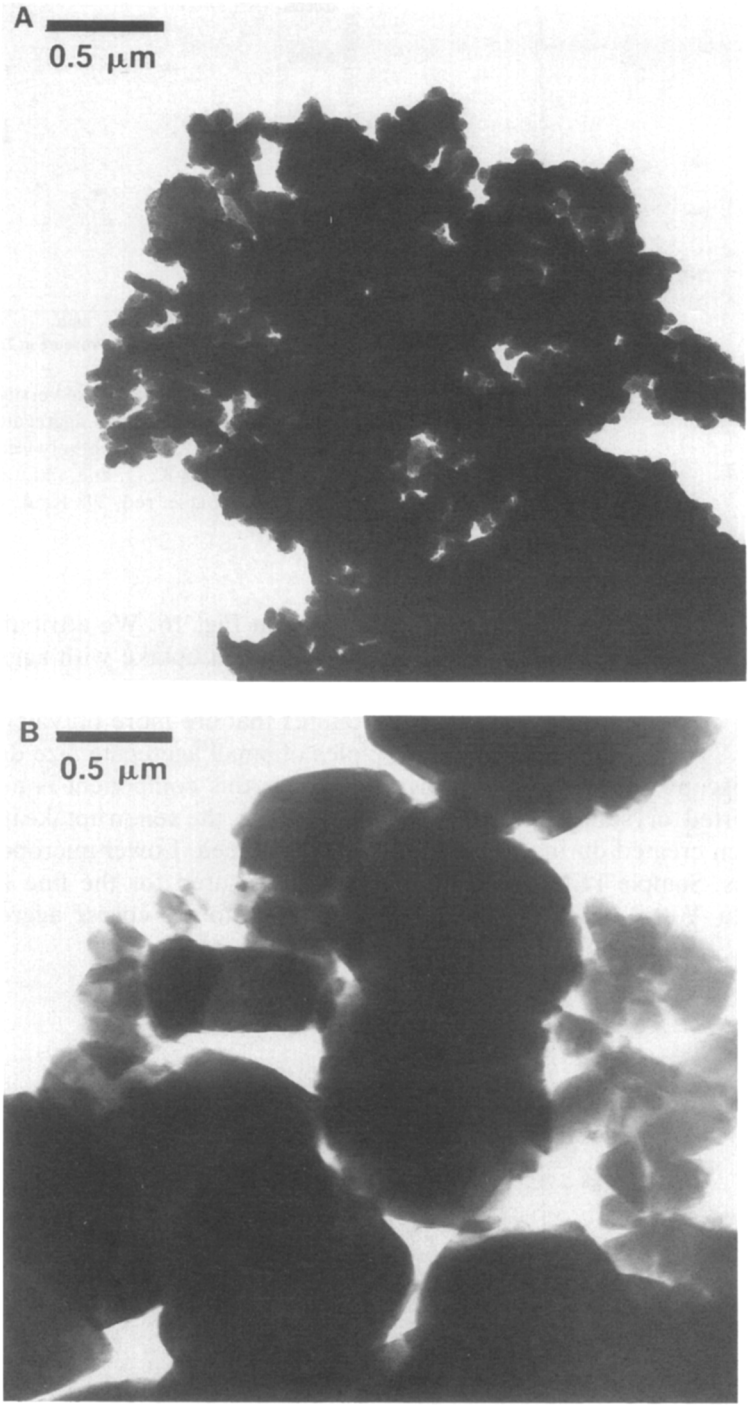

FIG. 16. Transmission electron micrographs of: (A) as-exchanged Ru–Y zeolite and (B) Na–Y zeolite

TABLE 2

Microporosity and Macroporosity Data

Zeolite	Microporosity (cc/g)	Macroporosity (cc/g)	Summed porosity (cc/g)	Total porosity (cc/g)
Crushed Na–Y	0.326	0.054	0.380	0.383
Coarse Na–Y	0.327	0.058	0.385	0.384
Medium Fe–Y	0.324	0.070	0.394	0.391
Supercoarse Fe–Y	0.325	0.065	0.390	0.393
Coarse Ru–Y	0.256	0.091	0.347	0.352
Fine Ru–Y	0.226	0.092	0.318	0.310

In addition, both of the Ru–Y samples have lower microporosity than the other samples studied (Table 2). The other zeolite samples studied have the same uptake regardless of aggregate size as indicated for Na–Y, Fe–Y, Ba–Y, and Ca–Y (Figs. 17–20).

DISCUSSION

To explain the differences in the ^{129}Xe NMR spectra of different particle size aggregates, the following model is proposed. True intracrystalline diffusion occurs very rapidly. The macroporous diffusion is slower, and the interaggregate diffusion is slower still, although the relative rates undoubtedly vary from sample to sample. Assuming that xenon in the interparticle void has a chemical shift very similar to that of gas phase xenon, the larger fraction of time xenon spends outside of the zeolite, the more shielded the observed chemical shift. In the fine aggregates a xenon atom must cross a greater number of grain boundaries during the NMR experiment. Surface diffusional barriers may well be present in these samples (*13*). Therefore, a larger fraction of time is spent in the void regions and the NMR signal appears farther upfield than the resonance of the coarse aggregate sample. This is observed in the Fe–Y, Ca–Y, and Ru–Y systems.

Packing a fine sample results in increasing aggregate contact and a decrease in grain boundaries. This is accompanied by a de-

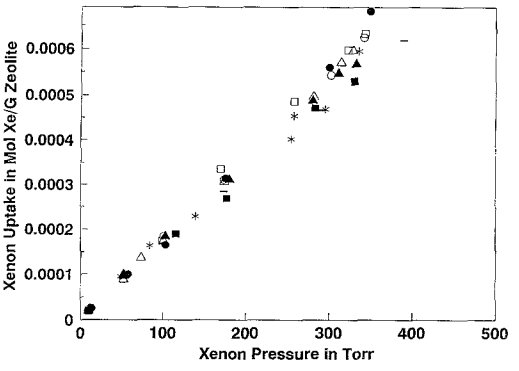

FIG. 18. Plot of xenon uptake versus xenon pressure for Fe–Y zeolites of various aggregate sizes and packing conditions (unless otherwise noted samples prepared by normal packing): –, coarse; *, medium; ●, fine; □, coarse, unpacked; ○, fine, unpacked; △, supercoarse, unpacked; ▲, supercoarse.

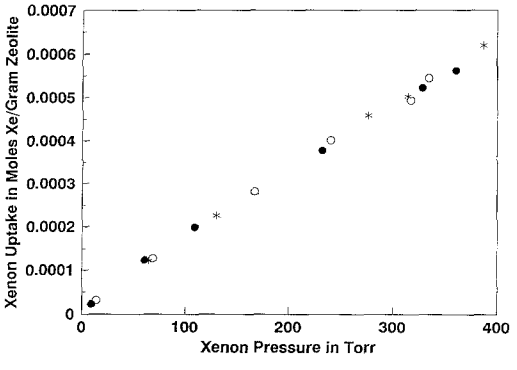

FIG. 17. Plot of xenon uptake versus xenon pressure for Na–Y zeolites of various aggregate sizes: ○, coarse; *, medium; ●, fine.

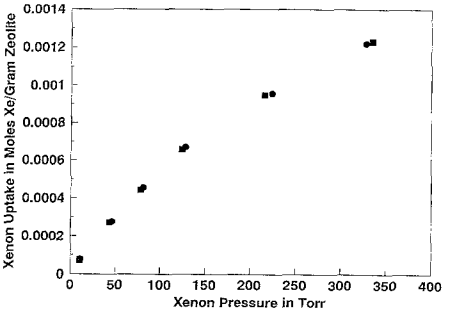

FIG. 19. Plot of xenon uptake versus xenon pressure for Ba–Y zeolites of various aggregate sizes: ■, coarse; ●, fine.

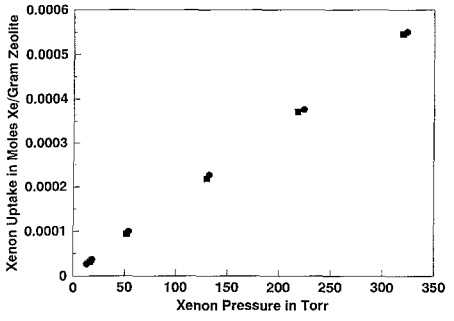

FIG. 20. Plot of xenon uptake versus xenon pressure for Ca–Y zeolites of various aggregate sizes: ●, coarse; ■, fine.

crease in void space. Packed fine samples, therefore, behave similarly to coarse aggregate unpacked samples.

The linewidth behavior observed in Fig. 6 is consistent with the same model. We see that fine aggregates of Na–Y have broader lines than coarse aggregates. Inside the Na–Y zeolite supercages the regions accessible to xenon are homogeneous because xenon encounters only oxygen and Na^+ cations. Furthermore, the supercages and channels of Na–Y are not well discriminated chemically from the exterior of the zeolite crystallites by ^{129}Xe NMR. It is clear that the shift in these systems is due almost solely to a change in mean free path or surface curvatures (*14–16*). As the aggregate size decreases xenon atoms spend a larger fraction of the time in the interaggregate mesopores. These mesopores have an inhomogeneous size distribution, resulting in a dispersion of xenon mean free paths and thus of chemical shifts. With larger aggregates, xenon is exposed less to the interaggregate grain boundary and experiences a more uniform environment.

As is evident from Figs. 7 and 8, the linewidths of Ru–Y and Fe–Y samples also depend on aggregate size. In these samples the fine aggregates are considerably narrower than the coarse aggregates, unlike in the Na–Y samples; however, in all cases the lines are broader than in Na–Y samples of either aggregate size. This behavior can also be ascribed to the macroscopic diffusion of xenon across grain boundaries. It is well known that contact of xenon with highly charged cations results in large chemical shifts. Within the zeolite crystals, one cannot expect uniformity of metal loading. Some xenon atoms will contact more metal cation sites than others. Because the chemical shifts associated with these sites are large, the shift dispersion should also be large. In the grain boundaries, however, the dispersion of shifts, while still present due to inhomogeneity of the mesopore volumes, is only of the size seen in the Na–Y samples. Thus, the more time a xenon spends in the mesopores at the grain boundaries, the more uniform its environment becomes. The Ca–Y and Ba–Y behave more similarly to the Na–Y zeolite than the Ru–Y and Fe–Y due to a higher concentration of exchanged cations. With higher exchanges, the zeolites are expected to have a more uniform metal loading. In addition, the exchange of transition metal ions may result in some structural damage resulting in a larger mesoporosity. This will be discussed further below.

Our model relies on the presence of mesopores at the zeolite aggregate grain boundaries. We investigated these mesopores via N_2 adsorption/desorption isotherms. A representative isotherm for Ru–Y fine is shown

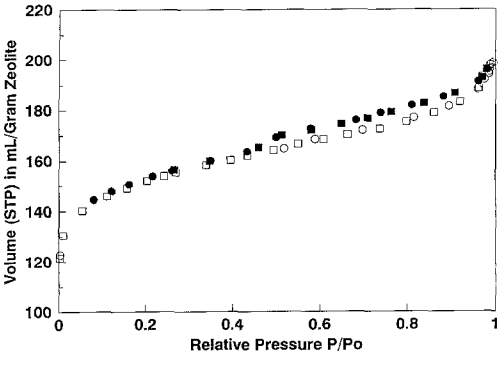

FIG. 21. Plot of nitrogen volume adsorbed versus relative nitrogen pressure for fine Ru–Y zeolite. Two separate cycles are shown: open symbols, adsorption; closed symbols, desorption.

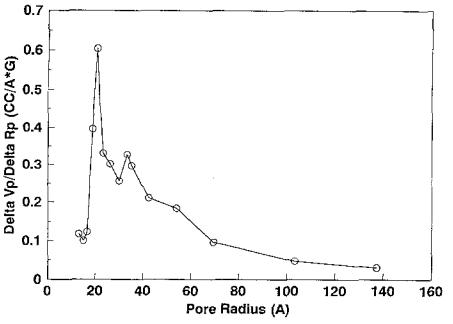

FIG. 22. Pore size distribution for supercoarse aggregates of Fe–Y zeolite.

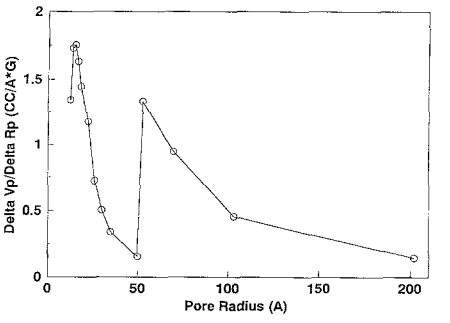

FIG. 24. Pore size distribution for crushed Fe–Y zeolite.

in Fig. 21. Reproducible hysteresis loops are exhibited. In both metal-exchanged samples, the hysteresis loops are much more pronounced than those observed in Na–Y in this study and by other workers (*17*). Despite the fact that these are Type I isotherms in the BET classification, the hysteresis can be attributed to capillary condensation, and thus the desorption loops can be used to calculate a pore size distribution (*18*). Several of these are shown in Figs. 22–24. The total pore volume of the "pores" present in this size range can be used to give an estimate of the macroporosity. These values are given in the first column of Table 2. It is likely that the macroporosity also reflects structural damage to the zeolite during ion exchange.

Nitrogen *t*-plots (*19*) were performed for several samples. The intercept of the linear region of the *t*-plots can be used to calculate the microporosity of the zeolite samples. These values are given in the second column in Table 2. The sum of the macroporosity and the microporosity should give the total porosity of the sample and the values for this are shown as well. Assuming all the pores are filled at a relative pressure greater than 0.95, then the total porosity can be calculated strictly from the adsorption isotherm. The values obtained using these two methods for these samples are in good agreement.

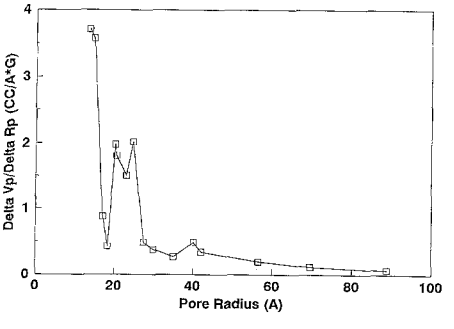

FIG. 23. Pore size distribution for coarse aggregates of Ru–Y zeolite.

To test the effect of particle size upon mixing experiments that had previously been performed, initially by our group and then by others, mixed samples of different aggregate sizes containing both Ru–Y and Na–Y were explored. Figures 25 and 26 show spectra of unreduced and reduced Ru–Y, respectively, for three different aggregate sizes. Interaggregate diffusion is more pronounced in the fine aggregate size samples, and, therefore, the peaks are somewhat merged as expected. In fact, for fine aggregates of reduced mixed Ru–Y/Na–Y samples the peaks are partially coalesced.

For mixed Ru–Y/Na–Y samples (Fig. 27) peaks associated with Ru–Y are shifted upfield relative to their position in unmixed samples. This is clear evidence of interaggregate diffusion. While there is very little movement of the upfield resonance after

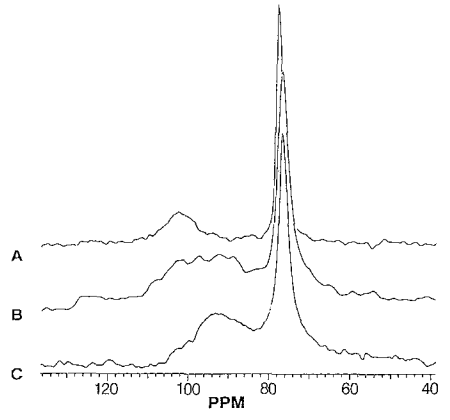

FIG. 25. ^{129}Xe NMR spectra for mixed Ru–Y/Na–Y zeolite samples of various aggregate sizes at xenon pressures of 194–199 Torr: (A) coarse, (B) medium, (C) fine.

mixing, the intensity of this resonance is decreasing. We expect that as the aggregate size is decreased, xenon will experience chemical exchange between resonance positions associated with its intracrystalline locations, both in Na–Y and Ru–Y aggregates, and the resonance position associated with the interparticle void region. We ascribe the upfield resonance to xenon in Na–Y crystallites *and* xenon in interaggregate voids. Exchange between sites within a Ru–Y aggregate and the interaggregate void in the fine samples will result in a coalescence of the line associated with xenon in Ru–Y and that of the interaggregate void regions. This will appear as an upfield shift in the resonance associated with xenon in Ru–Y and a decrease in the intensity of the line associated with the interparticle void regions and Na–Y. The similar exchange between sites within a Na–Y aggregate and the interaggregate voids results in no change in the xenon spectrum since these two regions have similar chemical shifts.

Complete coalescence of the ^{129}Xe NMR resonance is observed when the mixed Ru–Y/Na–Y sample is crushed in a mortar and pestle. In these samples there are far smaller aggregates and the aggregate contact is much greater. Thus, the motion of the xenon atom results in its sampling all three possible environments, Ru–Y crystallite, Na–Y crystallite, and interaggregate void volume. The chemical shift in the mixed sample lies halfway between the chemical shifts of the two unmixed samples (Fig. 28). Even at low temperatures the diffusion of xenon is rapid enough to coalesce the resonances, although the temperature dependence of the shift is different for the mixed and unmixed samples (Fig. 29).

CONCLUSION

Intercrystalline diffusion of xenon is an important factor in determining the ^{129}Xe

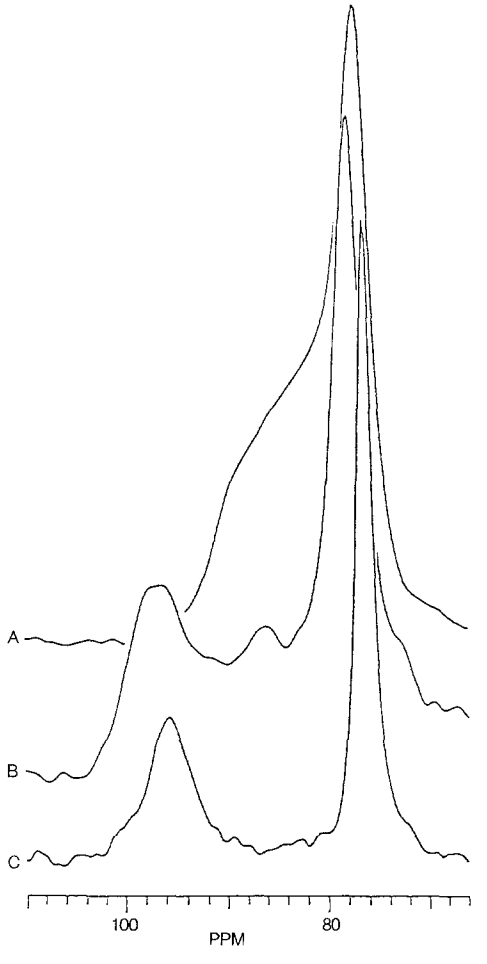

FIG. 26. ^{129}Xe NMR spectra of same samples as in Fig. 25 but reduced at room temperature. Xenon pressure 197–200 Torr. (A) fine, (B) medium, (C) coarse.

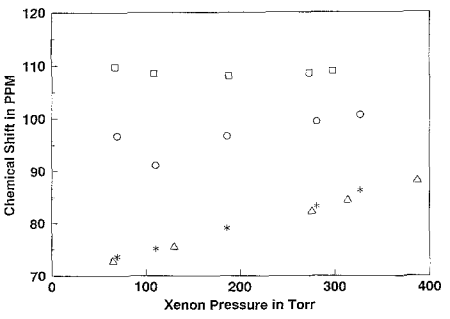

FIG. 27. Plot of xenon chemical shift versus xenon pressure for mixed and unmixed Ru–Y and Na–Y zeolites of medium aggregate size: □, Ru–Y/unmixed; △, Na–Y/unmixed; ○, Ru–Y/mixed; *, Na–Y/mixed.

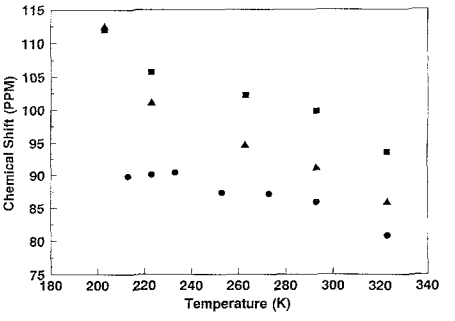

FIG. 29. Plot of xenon chemical shift versus acquisition temperature for mixed and unmixed Ru–Y and Na–Y zeolites: ■, Ru–Y/unmixed; ▲, Ru–Y and Na–Y/mixed; ●, Na–Y/unmixed. Samples with Ru–Y were reduced at 298 K.

NMR response in zeolites. Consideration of the xenon diffusion distance must be taken into account in studies of zeolites, particularly metal-exchanged zeolites. Estimations of the amount and range of heterogeneity of zeolite samples inferred from the observation of more than one ^{129}Xe resonance must take into account the diffusion distance of xenon. This is important in determination of whether heterogeneity is microscopic and exists within one zeolite crystal or is macroscopic, such as between the top and bottom of the NMR tube. The averaging of the NMR signal due to intercrystalline diffusion results in an aggregate-size dependency of the xenon chemical shift. We anticipate that the intercrystalline diffusional effects of xenon will be even more prevalent in systems having a greater degree of macroporosity such as silicas and aluminas.

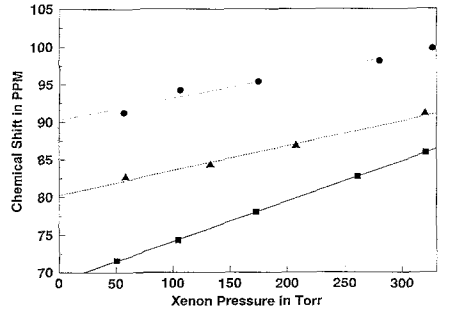

FIG. 28. Plot of xenon chemical shift versus xenon pressure for mixed and unmixed crushed Ru–Y and Na–Y zeolites: ■, Na–Y/unmixed; ▲, Ru–Y and Na–Y/mixed; ●, Ru–Y/unmixed. Samples with Ru–Y were reduced at 298 K.

ACKNOWLEDGMENTS

This work was supported by the National Science Foundation under Grant CHE8718850. This material is based upon work supported under a National Science Foundation Graduate Fellowship. We thank Prof. Robert DeAngelis and Christopher Reed for the electron microscopy work and Paul Molitor for the ^{27}Al NMR.

REFERENCES

1. Ito, T., and Fraissard, J., *J. Chem. Soc. Faraday Trans. 1* **83,** 451 (1987).
2. de Menorval, L. C., Raferty, D., Liu, S.-B., Takegoshi, K., Ryoo, R., and Pines, A., *J. Phys. Chem.* **94,** 27 (1990).
3. Shoemaker, R., and Apple, T., *J. Phys. Chem.* **91,** 4024 (1987).
4. Tsiao, C., Corbin, D. R., and Dybowski, C. R., *J. Phys. Chem.* **94,** 867 (1990).
5. Cheung, T. T. P., Fu, C. M., Wharry, S., *J. Phys. Chem.* **92,** 5170 (1988).
6. Karger, J., Pfeifer, H., Stallmach, F., and Spindler, H., *Zeolites* **10,** 288 (1990).
7. Springuel-Huet, M. A., Ito, T., and Fraissard, J. P., *in* "Structure and Reactivity of Modified Zeolites" (P. Jacobs, N. Jaeger, P. Jiru, V. Kazansky, and G. Schulz-Ekloff, Eds.), p. 13. Elsevier, Amsterdam, 1984.
8. Fraissard, J., Ito, T., de Menorval, L. C., and Springuel-Huet, M. A., *in* "Metal Microstructures in Zeolites" (P. Jacobs, N. Jaeger, P. Jiru, and G.

Schulz-Ekloff, Eds.), p. 179. Elsevier, Amsterdam, 1982.
9. Ryoo, R., Pak, C., and Chmelka, B. F., *Zeolites* **10,** 790 (1990).
10. Yang, O. B., Woo, S. I., and Ryoo, R., *J. Catal.* **123,** 375 (1990).
11. Corma, A., Fornes, V., Martin-Aranda, R. M., Garcia, H., and Primo, J., *Appl. Catal.* **59,** 237 (1990).
12. Jameson, A. K., Jameson, C. J., and Gutowsky, H. S., *J. Chem. Phys.* **53,** 2310 (1970).
13. Karger, J., Pfeifer, H., Stallmach, F., and Spindler, H., *Zeolites* **10,** 288 (1990).
14. Derouane, E. G., and Davis, M. E., *J. Mol. Cat.* **48,** 37 (1988).
15. Demarquay, J., and Fraissard, J., *Chem. Phys. Lett.* **136,** 314 (1987).
16. Derouane, E. G., and Nagy, J. B., *Chem. Phys. Lett.* **137,** 341 (1987).
17. Yoshida, A., Nakamoto, H., Okanishi, K., and Tsura, T. *Bull. Chem. Soc. Jpn.* **55,** 581 (1982).
18. Gregg, S. J., and Sing, K. S. W., "Adsorption, Surface Area and Porosity." Academic Press, London, 1982.
19. Cape, J. A., and Kibby, C. L., *J. Colloid Interface Sci.* **138,** 515 (1990).